Journal of Alloys and Compounds 639 (2015) 428–434

Contents lists available at ScienceDirect

Journal of Alloys and Compounds

journal homepage: www.elsevier.com/locate/jalcom

MWNT-supported bifunctional catalyst of β-FeOOH nanospindles for enhanced rechargeable Li–O_2 batteries

Jiaxin Li [a,b], Wen Weiwei [a], Mingzhong Zou [a], Lunhui Guan [b,*], Zhigao Huang [a,*]

[a] College of Physics and Energy, Fujian Normal University, Fujian Provincial Key Laboratory of Quantum Manipulation and New Energy Materials, Fuzhou, Fujian 350007, China
[b] State Key Laboratory of Structural Chemistry, Fujian Institute of Research on the Structure of Matter, Chinese Academy of Sciences, Fuzhou, Fujian 350002, China

ARTICLE INFO

Article history:
Received 17 September 2014
Received in revised form 15 January 2015
Accepted 9 March 2015
Available online 16 March 2015

Keywords:
Electrode materials
Energy storage materials
Nanofabrications
Electrochemical reactions

ABSTRACT

A novel composite of β-FeOOH nanospindles coated on multi-walled carbon nanotubes (β-FeOOH/MWNTs) has been synthesized *via* a wet chemical method and used as electrocatalysts for the cathodes of Li–O_2 batteries (LOBs). The β-FeOOH/MWNT cathodes can afford a high reversible capacity of 6000 mA h g^{-1} tested at 200 mA g^{-1} and cycle stability for 19 cycles with a reversible capacity of 600 mA h g^{-1} and good rate capability. The LOB performance should be benefited from the fast kinetics of electron transport through the MWNT support and the electro-catalytic activity provided by the β-FeOOH nanospindles. The preliminary result manifests that the composites of β-FeOOH/MWNTs are promising cathode electrocatalysts for LOBs.

1. Introduction

As a promising eco-friendly energy storage device, the Li–O_2 batteries (LOBs) delivered substantially higher energy density than conventional lithium batteries, has received extensive attention today [1–5]. It is believed that catalysts possessed high electrical conductivity and strong electro-catalytic activity, can significantly enhance oxygen reduction/evolution reactions (ORR/OER) and further improve the specific capacity and the cycling performance for LOBs [2–8]. Recently, tremendous effects have been devoted to develop cathode catalysts, mainly including functional doped-carbon materials [8,9], metal oxides [7,10,11], metal nitrides [12,13] and precious metals [14], etc. Among them, MnO_2-based catalysts reported for LOBs showed high reversible capacities with low ORR/OER overpotentials [10,15]. Especially, α-MnO_2, consisted of 2D edge-shared [MnO_6] octahedra layers with 2 × 2 tunnels, is beneficial for accommodation of Li^+ and O_2 ions within their inner tunnels, which enables the reversible formation/decomposition of Li_2O_2 [16–18]. Therefore, developing catalyst materials with such tunnel structure for LOBs is highly desired. Based on previous report [19], β-FeOOH exhibits a special 2 × 2 tunnel structure containing [$Fe^{3+}O_6$] octahedra, being similar to that of α-MnO_2. In addition, β-FeOOH can deliver high catalytic activity as a cathode catalyst for ORR in fuel cells, as well as an oxygen evolving photo-anode for water splitting [19,20]. Very recently, Kang et al. [21] studied a β-FeOOH nanorod bundles as a cathode catalyst for LOBs, exhibiting impressive catalytic activity, enabling excellent round-trip efficiency and enhanced cyclability. However, there are only a few reports on FeOOH catalysts investigated for LOBs. Since it is low-cost and easy to prepare, it is worth to develop FeOOH catalyst for LOBs.

Additionally, it is recognized that the carbon supports in the catalyst composites can offer facile and fast pathways to electrons for electrodes and preserve their initial structure with a high surface area for catalysts, thus improving catalytic activity and LOB performance [22–24]. Our previous work also proved this point of view [25]. Therefore, there is needed to design and fabricate carbon-supported FeOOH catalysts for high-performance LOBs. In this report, β-FeOOH nanospindles coated on multi-walled carbon nanotubes (β-FeOOH/MWNTs) were prepared *via* a wet chemical method. When employed β-FeOOH/MWNTs as catalyst for LOBs, the assembled cathodes exhibit good LOB performance with high specific capacity, good rate capability and cycle stability.

2. Experimental

2.1. Synthesis of β-FeOOH/MWNT composites

The MWNTs were purchased from Shenzhen Nanotech Port (Shenzhen, China) and used as received. According to previous report [26], 3 g of the MWNTs is refluxed in 90 mL of HNO_3 (65 wt.%) at 140 °C for 6 h. The acid treated MWNTs are rinsed with DI water until a neutral pH value is reached. Then they are collected

* Corresponding authors. Tel./fax: +86 591 83792835.
E-mail addresses: guanlh@fjirsm.ac.cn (L. Guan), zghuang@fjnu.edu.cn (Z. Huang).

http://dx.doi.org/10.1016/j.jallcom.2015.03.072
0925-8388/

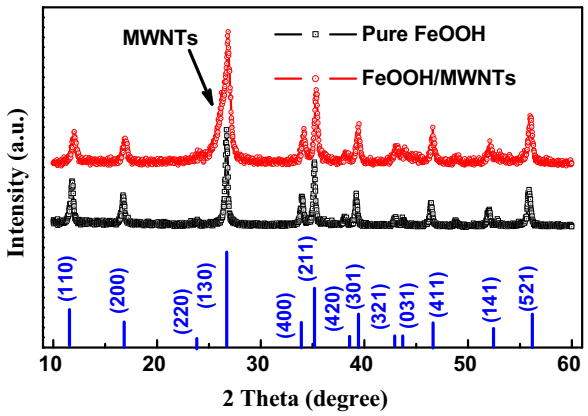

Fig. 1. XRD pattern of the pure β-FeOOH and β-FeOOH/MWNTs.

by filtration and dried at 80 °C for further use. After that, 30 mg of the MWNTs is dispersed in 10 mL of aqueous solution of 0.12 M $FeCl_3{\cdot}6H_2O$ by ultra-sonication for 30 min in a capped bottle. After thorough mixing, the suspension is kept in an oil bath under stirring at 75 °C for 8 h. The final products are collected by several centrifugation (2000 rpm) cycles before drying at 80 °C for 24 h. The pure β-FeOOH composite was synthesized without adding MWNTs.

2.2. Sample characterization

The structure and morphology of the obtaining composites were characterized by X-ray diffraction (XRD, RIGAKU SCXmini), Raman spectroscopy (Renishaw, excited at 514.5 nm), transmission electron microscopy (TEM, Tecnai G2 F20) and energy dispersive X-ray spectroscopy (EDS).

2.3. Electrochemical measurements

According to our previous report [25], the electrochemical behaviors were measured in a Swagelok cell with a 0.5 cm^2 hole placed on the cathode side to enable oxygen flow in. All the batteries were assembled in a dry argon-filled glove box. The working electrodes were prepared by mixing 60 wt.% carbon active material (ketjen black, KB), 30 wt.% electrocatalysts of β-FeOOH/MWNTs or pure β-FeOOH, and 10 wt.% polyvinylidene difluoride (PVDF). The loading ratio of active material is about 1.6–2.0 mg cm^{-2} per electrode. The capacity for LOBs is calculated based on the weight of KB. And then a commercially available electrolyte solution of 1 M LITFSI (Lithium bis(trifluoromethanesulfonyl) imide) in TEGDME (Tretraethylene glycol dimethyl ether) was impregnated into a glass fiber membrane and sandwiched between a lithium metal anode and air cathode. The batteries were cycled by LAND 2001A at room temperature with a lower voltage limit of 2.0 V and an upper limit of 4.3 V versus Li^+/Li at different conditions after a 2–3 h

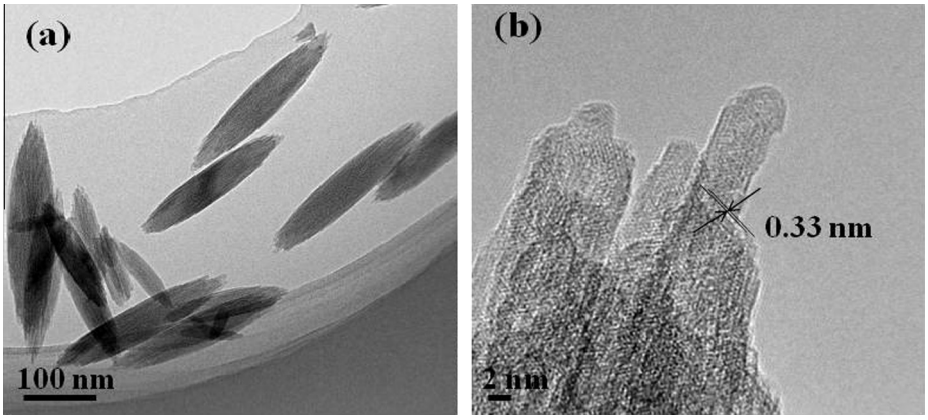

Fig. 2. TEM and HR-TEM images of pure β-FeOOH.

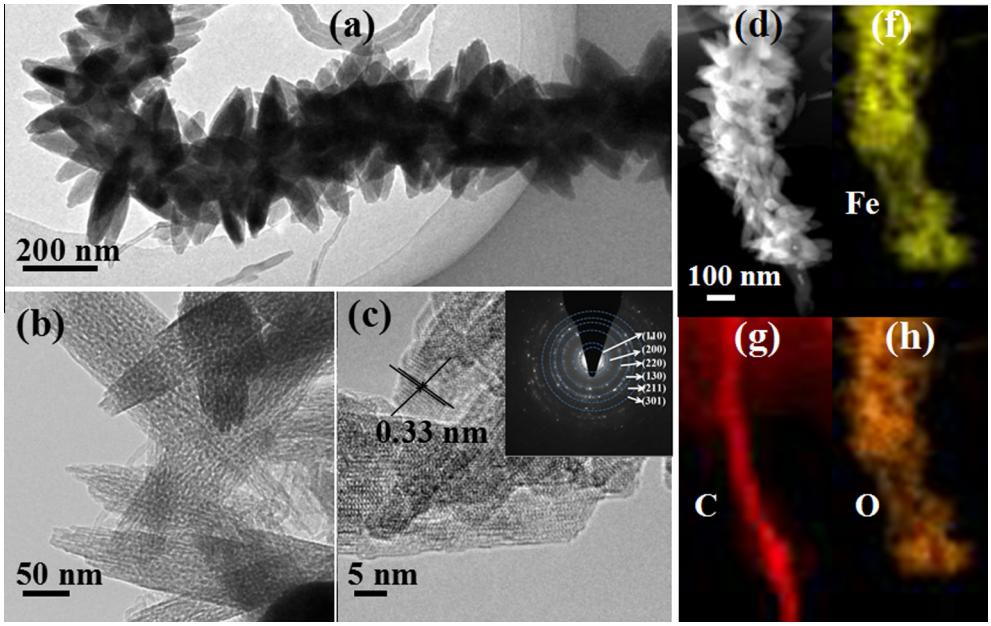

Fig. 3. (a)–(c), TEM, HR-TEM images and the corresponding SAED pattern of the β-FeOOH/MWNTs; STEM image (d) and iron (f), carbon (g), and oxygen (h) element mapping images of β-FeOOH/MWNTs.

rest period. Cyclic voltammetry (CV) test was operated on a CHI660D Electrochemical Workstation with a rate of 0.20 mV s^{-1}. Electrochemical impedance spectra (EIS) was carried out by applying an AC voltage of 5 mV over the frequency range from 1 mHz to 100 kHz.

3. Results and discussion

The pure β-FeOOH and β-FeOOH/MWNTs were characterized by XRD recorded in the range of 2θ from 10° to 60°, as shown in Fig. 1. The main diffraction peaks for β-FeOOH and β-FeOOH/MWNTs were both well indexed to the (110), (200), (130), (222), (400), (422) and (440) planes of β-FeOOH (JCPDF No. 75-1594) [27]. An additional abroad peak around 26° for β-FeOOH/MWNTs resulted from the MWNTs. The peaks are relatively sharp in the XRD, corresponding to well crystallization of the primary β-FeOOH particles. This result is consistent with the following TEM observation.

The morphology and structure of pure β-FeOOH and β-FeOOH/MWNTs were further detected by TEM, HR-TEM and element mapping analysis, respectively. As seen from Fig. 2(a), the TEM image shows β-FeOOH nanospindles with lengths from 150 to 250 nm and diameters of 20–60 nm. Clear lattice fringes for β-FeOOH was observed in Fig. 2(b), showing the regular interplanar spacing of ~0.33 nm for the (130) planes. Fig. 3(a) and (b), reveal that β-FeOOH nanospindles radial assembled on the curvature of MWNT backbones. The corresponding SAED pattern shown in Fig. 3(c) demonstrates the crystalline nature of β-FeOOH/MWNTs. The diffraction rings are related to the (110), (200), (130), (211) and (301) planes for β-FeOOH [26]. Element mapping analysis was used to further confirm the structure and composition of β-FeOOH/MWNTs. Fig. 3(d)–(h) show that Fe and O elements in the sample are homogeneously distributed in the composite, indicating the FeOOH nanospindles are homogeneously distributed around the MWNTs. Thus, it is supposed that the catalytic active sites from FeOOH should be utilized, thereby improving the electrochemical activity for the assembled LOBs.

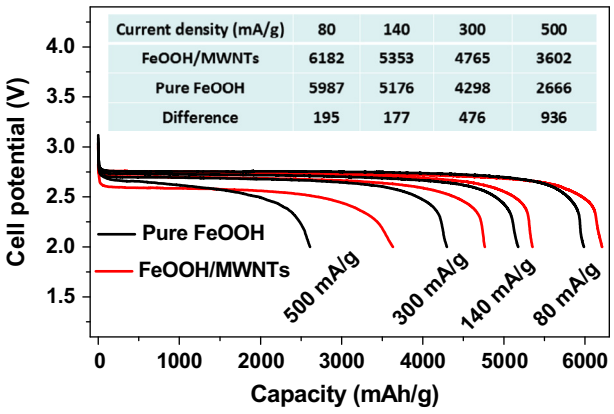

Fig. 5. The discharge curves at different current densities for both of pure β-FeOOH and β-FeOOH/MWNT electrodes. The inset table shows the comparison of discharge capacities between β-FeOOH and β-FeOOH/MWNT electrodes.

As shown in Fig. 4, the electrochemical properties related to cyclic voltammetry (CV) curves and discharge–charge (D–C) characteristic have been carried out to explore the application of the KB and β-FeOOH/MWNTs as catalysts in cathodes for LOBs. A featureless CV curve shown in Fig. 4(a) for pure KB cathode is observed in its OER process. But for β-FeOOH/MWNTs shown in Fig. 4(c), the anodic peak appearing near 3.5 V is related to the oxygen evolution by the oxidation of lithium peroxide [5,18]. Moreover, in the ORR scan, KB cathode exhibits a slightly lower ORR onset potential in the first cycle and lower peak currents than β-FeOOH/MWNT cathode in the following cycles. These results indicate that the ORR/OER reactions are catalytically sensitive and can be enhanced by

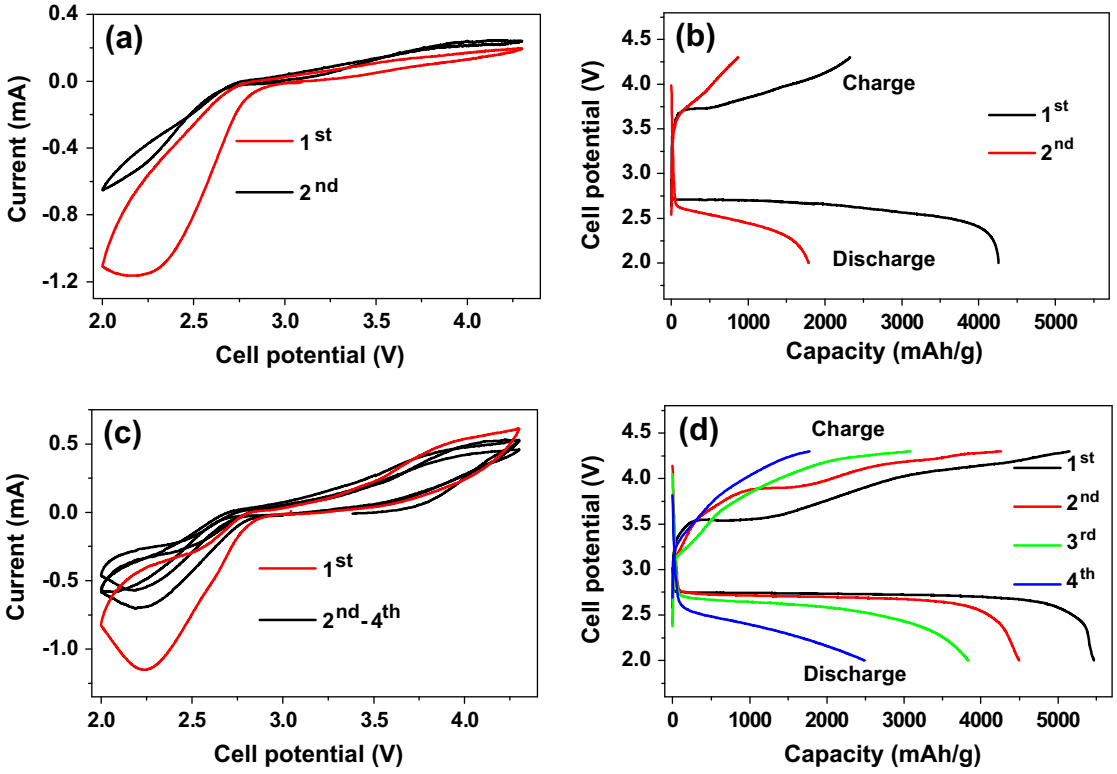

Fig. 4. Cyclic voltammetry curves of (a) pure KB and (c) β-FeOOH/MWNT electrodes; discharge–charge characteristic of (b) pure KB and (d) β-FeOOH/MWNT electrodes at 200 mA/g.

introducing β-FeOOH/MWNT catalyst. Fig. 4(b) and (d) compare the initial D–C characteristic of pure KB and β-FeOOH/MWNT electrodes for LOBs. The potential difference for β-FeOOH/MWNT electrode was ~1.10 V, being lower than that of 1.40 V for the KB electrode. These results are similar to the previous reports [28,29]. In addition, the LOB with β-FeOOH/MWNT catalyst shows a much higher specific capacity and better reversibility than those of pure KB.

To evaluate the MWNT effect on the LOB performance, the D–C characteristic of pure β-FeOOH and β-FeOOH/MWNT cathodes under different current densities has been investigated in Fig. 5. The discharge voltage and specific capacity for both of pure β-FeOOH and β-FeOOH/MWNT electrodes decrease with increased current density. This phenomenon should be caused by significant chemical polarization at higher current densities. Meanwhile, it is noticeable that the catalyst with MWNT support exhibits larger capacity retention than pure β-FeOOH. As shown in the inset of Fig. 5, the β-FeOOH/MWNT electrode delivered specific capacities of 3602 mA h g^{-1}, which value is much larger than that of 2666 mA h g^{-1} for pure β-FeOOH tested at 500 mA g^{-1}. Thus, the MWNTs can significantly lead to a low electrode interface polarization.

Fig. 6 shows the cycle stability for β-FeOOH and β-FeOOH/MWNT electrodes tested with a restriction of the capacity to 550 mA h g^{-1} at 200 mA g^{-1}. As disclosed in Fig. 6(a) and (b), the β-FeOOH/MWNT electrode exhibits better capacity retention for 19 cycles than that of 15 cycles for β-FeOOH. Meanwhile, the trend of decreasing in the cutoff voltage for discharged process and increasing in the cutoff voltage for charged process for these two electrodes is shown Fig. 6(c). The cutoff voltage of 2.5 V at the 16th cycle for β-FeOOH/MWNT electrode still remains acceptable. However, there is a significant drop in the cutoff voltage for discharged process from the 12th cycle for the β-FeOOH electrode.

As we know, Raman spectroscopy is one of the most useful techniques for measuring Li_2O_2 materials during discharge/charge in the LOBs [30]. Fig. 7 shows Raman spectra of the β-FeOOH/MWNT electrodes between 100 and 1100 cm^{-1}. According to the previous reports [30,31], main features of the wave-number observed at about 375, 388, 410, 519, 625 and 698 cm^{-1} for flesh β-FeOOH crystalline can be found in Fig. 7(a). After the first discharge to 2.0 V, the Raman pattern shown in Fig. 7(b) reveals that Li_2O_2 was observed as the major discharge product in the β-FeOOH/MWNT electrode (marked with blue arrow). Meanwhile, as shown in Fig. 7(c), the Raman result recharged up to a potential of 4.3 V shows no Li_2O_2 discharge product, while some additional peaks for β-FeOOH re-appear. Thus, these results indicate that the ORR/OER reactions are reversible and catalytically sensitive enhanced by β-FeOOH/MWNTs. Meanwhile, after discharge with a restricting capacity of 550 mA h g^{-1} for 20 cycles, all weakened

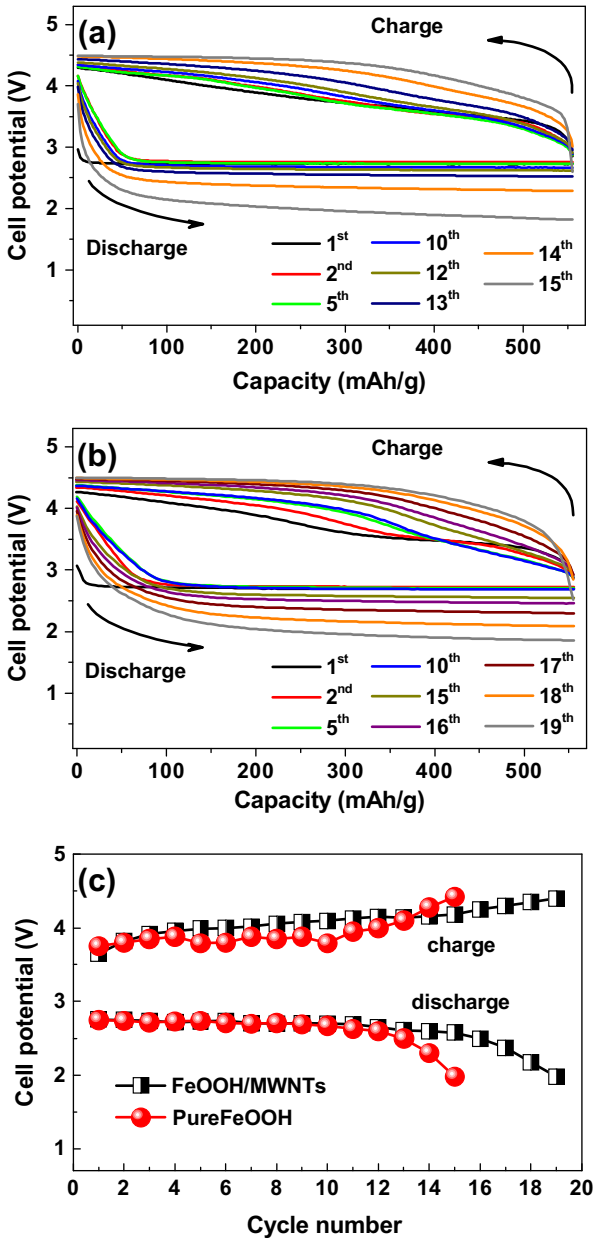

Fig. 6. Cycling performance of (a) β-FeOOH and (b) β-FeOOH/MWNT electrodes at 200 mA g^{-1} with a restricting capacity of 550 mA h g^{-1}; (c) the comparison of charge and discharge potential plateaus between β-FeOOH and β-FeOOH/MWNT electrodes.

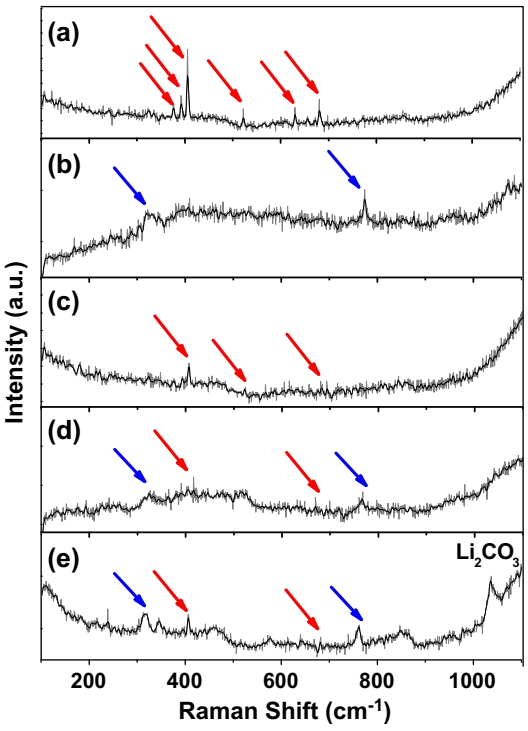

Fig. 7. The Raman spectra of β-FeOOH/MWNT electrodes: (a) before test, (b) after first discharge to 2.0 V, (c) after first recharge to 4.3 V, (d) after discharge with a restricting capacity of 550 mA h g^{-1} for 20 cycles and (e) after 10 D–C cycles between 2.0 and 4.3 V.

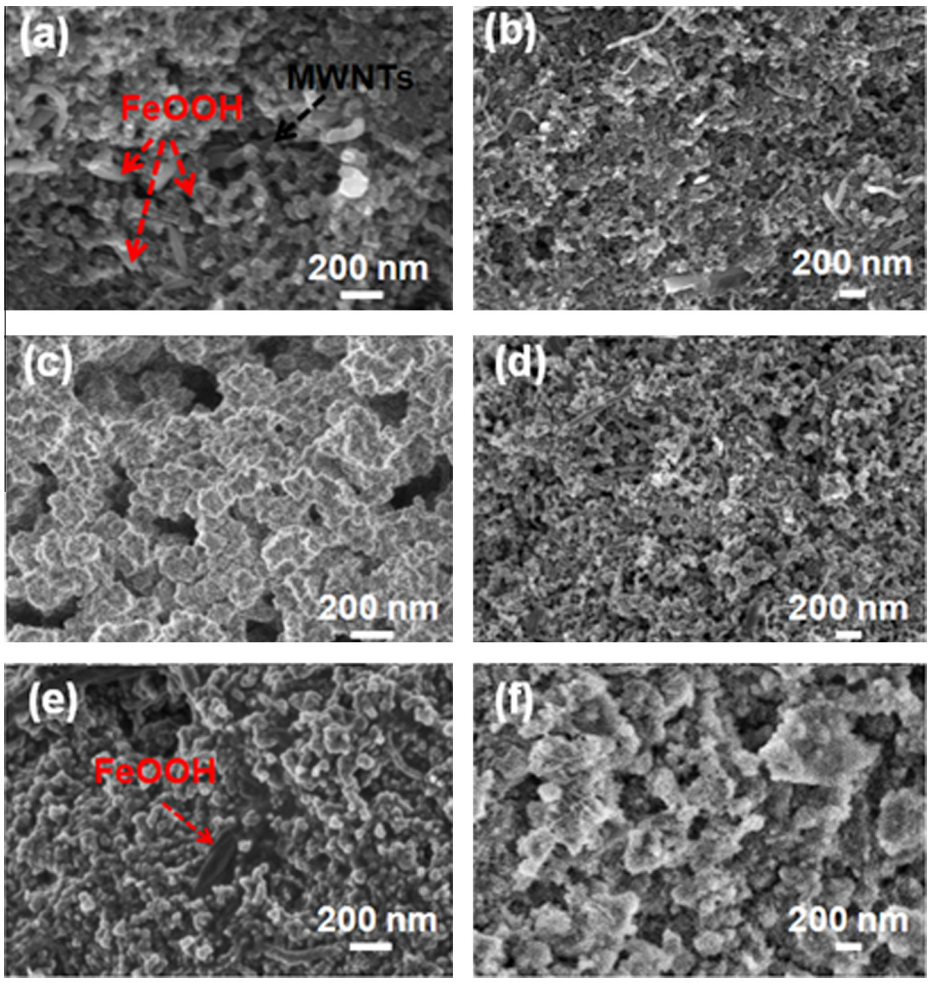

Fig. 8. SEM images of β-FeOOH/MWNT electrodes: (a and b) before test, (c) after the 1st discharge to 2.0 V, (d) after the 1 st recharge to 4.3 V, (e) after discharge with a restricting capacity of 550 mA h g^{-1} for 20 cycles and (f) after 10 D–C cycles between 2.0 and 4.3 V.

Raman peaks shown in Fig. 7(d) for both Li_2O_2 and β-FeOOH can be observed clearly, revealing that minor un-decomposition of Li_2O_2. However, after 10 D–C cycles between 2.0 and 4.3 V, all the clear peaks shown in Fig. 7(e) for Li_2O_2 and β-FeOOH, as well as an additional peak of Li_2CO_3 can be found. Thus, Li_2O_2 intermingled with some Li_2CO_3 are the dominant discharge products for LOBs and their formation/decomposition appear to be un-reversible after long D–C cycles leading to the capacity fading.

The SEM was used to analyze the products after different test conditions and further explore the insights of the LOB D–C process. The SEM images for pristine β-FeOOH/MWNT cathodes shown in Fig. 8(a) and (b), clearly present many β-FeOOH/MWNT composite and KB nanospheres. Fig. 8(c) shows that the corresponding the 1st discharged products were deposited on the electrode after discharge. Then after the 1st recharge, the products disappear and a relatively clean electrode is observed in Fig. 8(c). These findings revealed that the cathode could enable the reaction of "$2Li^+ + 2e^- + O_2 \leftrightarrow Li_2O_2$" to remain reversible during the ORR and OER processes. This result is consistent to the Raman result. Further combined with the above Raman result, after discharging with a restricting capacity of 550 mA h g^{-1} for 20 cycles, some residual coating products still remain in Fig. 8(e), revealing minor un-decomposition of Li_2O_2 [32,33]. Compared with Fig. 8(e), the materials of β-FeOOH/MWNT and KB from electrode cannot be found in Fig. 8(f). After 10 D–C cycles between 2.0 and 4.3 V shown in Fig. 8(f), the obvious close-packed layer of discharged products were deposited on the electrode surface. As noted above, the degradation for LOB performance should be due to the deposition of reaction products in the pores which blocks the oxygen pathway or due to the deposition of products on the catalytic active sites that reduces the activity of the catalyst.

Electrochemical impedance spectroscopy (EIS) is a highly resolved electro-analytical technique that may provide unique information about the nature of electrode process related to a wide range of time constants [34]. Fig. 9 presents EIS profiles of β-FeOOH/MWNT electrodes before and after different test conditions and their corresponding equivalent circuits. The overall shape of Nyquist plots for these two electrodes are composed of three parts, essentially high and middle frequency intercept of the semicircle followed by a one line. According to the literature [35], the high frequency intercept of the semicircle on the real axis was reflected by an ohmic resistance (R_1), which includes ionic resistance from the separator paper and electrical resistance between the electrode and the current collector. The depressed semicircle at middle frequency was contributed by a parallel combination of charge-transfer resistance (R_2), corresponding to the kinetic reaction at the air electrode surface. The linear spike at low frequency could be described by a finite length Warbury element R_W. According to the corresponding equivalent circuits shown in the insets of Fig. 9, the R_1 values for pristine electrodes are similar to those cases of after restricting D–C process and after 10 D–C cycles between 2.0 and 4.3 V shown in Fig. 9, indicating there are no obvious decomposition reacted in electrolyte. Besides, the R_2 value of 680 Ω after 20 cycles of the restricting D–C process is obviously

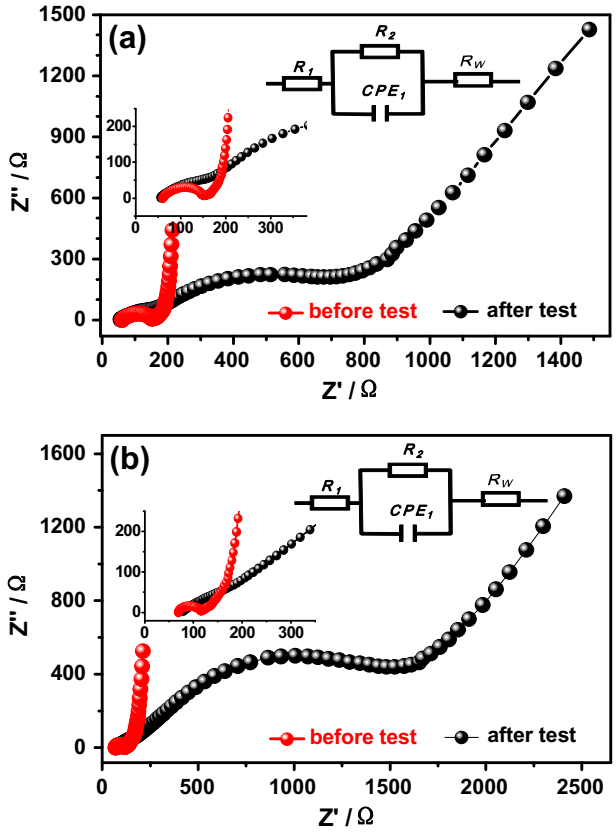

Fig. 9. The EIS profiles of β-FeOOH/MWNT electrodes: (a) before and after discharge with a restricting capacity of 550 mA h g^{-1} for 20 cycles and (b) before and after 10 D–C cycles between 2.0 and 4.3 V. Both insets show the corresponding equivalent circuits.

smaller than 1550 Ω after 10 D–C cycles between 2.0 and 4.3 V, suggesting the electrode after 10 D–C cycles between 2.0 and 4.3 V presents a thicker coating product of ORR/OER reactions. This phenomenon is consistent the above-analysis for SEM results. Thus, the capacity fading in LOBs may be mainly from accumulation of the ORR/OER reaction products such as Li_2O_2 and Li_2CO_3. Certainly, obtaining good LOB performance is also dependent on other critical technological strategies such as fabricating cathodes with effective microstructures. At least, it can be concluded from this work that the β-FeOOH/MWNTs are promising electro-catalysts for LOBs.

4. Conclusion

In this work, a wet chemical method has been developed for preparing bifunctional catalysts of β-FeOOH/MWNTs for LOBs. Owing to their favorable structures and desirable bifunctional catalytic activities, the resulting β-FeOOH/MWNT cathodes delivered better LOB battery performance than pure β-FeOOH nanospindles. It is believed that the fast kinetics of electron transport provided by the MWNT support and the electro-catalytic activity provided by the β-FeOOH nanospindles can benefit the performance of LOBs. The preliminary result manifests that the composites of β-FeOOH/MWNTs are promising cathode electro-catalysts for LOBs.

Acknowledgements

We acknowledge the financial support by the Natural Science Foundations of China (No. 21203025), Science and Technology Major Projects of Fujian Province (2013HZ0003) and Project of Fujian Development and Reform Commission (2013-577).

References

[1] F. Cheng, J. Chen, Metal–air batteries: from oxygen reduction electrochemistry to cathode catalysts, Chem. Soc. Rev. 41 (2012) 2172–2192.
[2] M. Balaish, A. Kraytsberg, Y. Ein-Eli, A critical review on lithium–air battery electrolytes, Phys. Chem. Chem. Phys. 16 (2014) 2801–2822.
[3] C. Jin, Z. Yang, X. Cao, F. Lu, R. Yang, A novel bifunctional catalyst of $Ba_{0.9}Co_{0.5}Fe_{0.4}Nb_{0.1}O_{3-\delta}$ perovskite for lithium–air battery, Int. J. Hydrogen Energy 39 (2014) 2526–2530.
[4] A. Riaz, K.N. Jung, W. Chang, S.B. Lee, T.H. Lim, S.J. Park, R.H. Song, S. Yoon, K.H. Shin, J.W. Lee, Carbon-free cobalt oxide cathodes with tunable nanoarchitectures for rechargeable lithium–oxygen batteries, Chem. Commun. (Camb) 49 (2013) 5984–5986.
[5] Z.L. Wang, D. Xu, J.J. Xu, X.B. Zhang, Oxygen electrocatalysts in metal–air batteries: from aqueous to nonaqueous electrolytes, Chem. Soc. Rev. (2013).
[6] Q. Li, P. Xu, B. Zhang, H. Tsai, J. Wang, H.L. Wang, G. Wu, One-step synthesis of Mn_3O_4/reduced graphene oxide nanocomposites for oxygen reduction in nonaqueous Li–O_2 batteries, Chem. Commun. (Camb) 49 (2013) 10838–10840.
[7] K. Guo, Y. Li, J. Yang, Z. Zou, X. Xue, X. Li, H. Yang, Nanosized Mn–Ru binary oxides as effective bifunctional cathode electrocatalysts for rechargeable Li–O_2 batteries, J. Mater. Chem. A 2 (2014) 1509.
[8] H. Nie, H. Zhang, Y. Zhang, T. Liu, J. Li, Q. Lai, Nitrogen enriched mesoporous carbon as a high capacity cathode in lithium–oxygen batteries, Nanoscale 5 (2013) 8484–8487.
[9] C.-H. Ahn, R.S. Kalubarme, Y.-H. Kim, K.-N. Jung, K.-H. Shin, C.-J. Park, Graphene/doped ceria nano-blend for catalytic oxygen reduction in non-aqueous lithium–oxygen batteries, Electrochim. Acta 117 (2014) 18–25.
[10] X. Hu, X. Han, Y. Hu, F. Cheng, J. Chen, Epsilon-MnO_2 nanostructures directly grown on Ni foam: a cathode catalyst for rechargeable Li–O_2 batteries, Nanoscale 6 (2014) 3522–3525.
[11] Y. Li, L. Zou, J. Li, K. Guo, X. Dong, X. Li, X. Xue, H. Zhang, H. Yang, Synthesis of ordered mesoporous $NiCo_2O_4$ via hard template and its application as bifunctional electrocatalyst for Li–O_2 batteries, Electrochim. Acta 129 (2014) 14–20.
[12] J.L. Shui, N.K. Karan, M. Balasubramanian, S.Y. Li, D.J. Liu, Fe/N/C composite in Li–O_2 battery: studies of catalytic structure and activity toward oxygen evolution reaction, J. Am. Chem. Soc. 134 (2012) 16654–16661.
[13] J. Park, Y.-S. Jun, W.-R. Lee, J.A. Gerbec, K.A. See, G.D. Stucky, Bimodal mesoporous titanium nitride/carbon microfibers as efficient and stable electrocatalysts for Li–O_2 batteries, Chem. Mater. 25 (2013) 3779–3781.
[14] G. Zhao, J. Lv, Z. Xu, L. Zhang, K. Sun, Carbon and binder free rechargeable Li–O_2 battery cathode with Pt/Co_3O_4 flake arrays as catalyst, J. Power Sources 248 (2014) 1270–1274.
[15] A.K. Thapa, B. Pandit, H.S. Paudel, R. Thapa, S. Ida, J.B. Jasinski, G.U. Sumanasekera, T. Ishihara, Polythiophene mesoporous birnessite-MnO_2/Pd cathode air electrode for rechargeable Li–Air battery, Electrochim. Acta 127 (2014) 410–415.
[16] X. Wang, Y. Li, Rational synthesis of α-MnO_2 single-crystal nanorods, Chem. Commun. (2002) 764–765.
[17] A. Débart, J. Bao, G. Armstrong, P.G. Bruce, An O_2 cathode for rechargeable lithium batteries: the effect of a catalyst, J. Power Sources 174 (2007) 1177–1182.
[18] A. Débart, A.J. Paterson, J. Bao, P.G. Bruce, A-MnO_2 nanowires: a catalyst for the O_2 electrode in rechargeable lithium batteries, Angew. Chem. Int. Ed. 47 (2008) 4521–4524.
[19] J.A. Seabold, K.-S. Choi, Efficient and stable photo-oxidation of water by a bismuth vanadate photoanode coupled with an iron oxyhydroxide oxygen evolution catalyst, J. Am. Chem. Soc. 134 (2012) 2186–2192.
[20] K.N. Zhu, H.Y. Qin, B.H. Liu, Z.P. Li, Carbon nanotubes supported Fe-based compounds as the electrode catalyst for oxygen reduction reaction, J. Power Sources 196 (2011) 182–185.
[21] J. Jung, K. Song, D.R. Bae, S.W. Lee, G. Lee, Y.-M. Kang, β-FeOOH nanorod bundles with highly enhanced round-trip efficiency and extremely low overpotential for lithium–air batteries, Nanoscale 5 (2013) 11845–11849.
[22] C. Sun, F. Li, C. Ma, Y. Wang, Y. Ren, W. Yang, Z. Ma, J. Li, Y.-J. Chen, Y. Kim, L. Chen, Graphene–Co_3O_4 nanocomposite as an efficient bifunctional catalyst for lithium–air batteries, J. Mater. Chem. A 2 (2014) 7188–7196.
[23] X. Lin, L. Zhou, T. Huang, A. Yu, Hierarchically porous honeycomb-like carbon as a lithium–oxygen electrode, J. Mater. Chem. A 1 (2013) 1239–1245.
[24] W.-H. Ryu, T.-H. Yoon, S.H. Song, S. Jeon, Y.-J. Park, I.-D. Kim, Bifunctional composite catalysts using Co_3O_4 nanofibers immobilized on nonoxidized graphene nanoflakes for high-capacity and long-cycle Li–O_2 batteries, Nano Lett. 13 (2013) 4190–4197.
[25] J. Li, N. Wang, Y. Zhao, Y. Ding, L. Guan, MnO_2 nanoflakes coated on multi-walled carbon nanotubes for rechargeable lithium–air batteries, Electrochem. Commun. 13 (2011) 698–700.
[26] Z. Wang, D. Luan, S. Madhavi, Y. Hu, X.W. Lou, Assembling carbon-coated α-Fe_2O_3 hollow nanohorns on the CNT backbone for superior lithium storage capability, Energy Environ. Sci. 5 (2012) 5252–5256.
[27] C. Lei, F. Han, Q. Sun, W.-C. Li, A.-H. Lu, Confined nanospace pyrolysis for the fabrication of coaxial Fe_3O_4@C hollow particles with a penetrated

mesochannel as a superior anode for Li–Ion batteries, Chem. – A Eur. J. 20 (2014) 139–145.
[28] J. Li, M. Zou, L. Chen, Z. Huang, L. Guan, An efficient bifunctional catalyst of Fe/Fe_3C carbon nanofibers for rechargeable Li–O_2 batteries, J. Mater. Chem. A 2 (2014) 10634.
[29] J. Li, M. Zou, W. Wen, Y. Zhao, Y. Lin, L. Chen, H. Lai, L. Guan, Z. Huang, Spinel MFe_2O_4 (M = Co, Ni) nanoparticles coated on multi-walled carbon nanotubes as electrocatalysts for Li–O_2 batteries, J. Mater. Chem. A 2 (2014) 10257.
[30] O. Sei, D. Cook, H. Townsend, Characterization of iron oxides commonly formed as corrosion products on steel, Hyperfine Interact. 12 (1998) 59–66.
[31] H. Song, L. Liu, X. Jia, C. Min, Synthesis of multi-walled carbon nanotubes/β-FeOOH nanocomposites with high adsorption capacity, J. Nanopart. Res. 14 (2012) 1290–1297.
[32] M. Ottakam, S. Freunberger, Z. Peng, P. Bruce, The carbon electrode in nonaqueous Li–O_2 cells, J. Am. Chem. Soc. 135 (2013) 494–500.
[33] S. Freunberger, Y. Chen, N. Drewet, L. Hardwick, B. Fanny, P. Bruce, The lithium–oxygen battery with ether-based electrolytes, Angew. Chem. Int. Ed. 50 (2011) 8609–8613.
[34] J. Li, M. Zou, Y. Zhao, Y. Lin, H. Lai, L. Guan, Z. Huang, Coaxial MWNTs@MnO_2 confined in conducting PPy for kinetically efficient and long-term lithium ion storage, Electrochim. Acta 111 (2013) 65–171.
[35] H. Kitaura, H. Zhou, Electrochemical performance of solid-state lithium–air batteries using carbon nanotube catalyst in the air electrode, Adv. Energy Mater. 2 (2012) 889–894.